Temperature effects in the electronic shells and supershells of lithium clusters

C. Bréchignac, Ph. Cahuzac, F. Carlier, M. de Frutos, and J. Ph. Roux
Laboratoire Aimé Cotton, Université Paris–Sud, Bâtiment 505, 91405 Orsay CEDEX, France
(Received 8 June 1992; revised manuscript received 31 August 1992)

Mass-abundance spectra of isotopically enriched lithium clusters from a gas aggregation source have been recorded for several laser flux densities of the ionizing laser. Shell and supershell structures are clearly observed. Thermal effects are put into evidence which tend to smooth out the shell structure of large masses. At the lowest temperature sharp features are revealed in the node and antinode regions of the beating supershell pattern. These structures are discussed in the light of theoretical models, and compared to other alkalis.

I. INTRODUCTION

For several years, most of the properties of metallic clusters have been understood in terms of their electronic structure. Assuming that the valence electrons form a quantized Fermi gas confined in a spherical potential well, electronic shell structure is obtained with shell closing at electron numbers $N=2,8,20,34,40,58,92,\ldots$.[1,2] It has been shown that electronic shell structure governs the ionization potentials,[3,4] static polarizabilities,[5] binding energies,[6,7] and consequently the relative abundance in metal cluster beams such as alkalis,[8,9] copper, silver, gold,[10–13] and, recently, aluminum.[14]

Recent calculations developed by Nishioka, Hansen, and Mottelson[15] on electronic shell structure of large sodium clusters up to 3000 atoms pointed out "supershell structure" in the level density and the total electronic binding energies. Following the idea of Balian and Bloch,[16] such a supershell structure is interpreted in terms of a beating pattern of level density due to the superposition of amplitudes associated with triangular and squared classical orbits of the valence electrons. In fact, the location of the shells and supershells depends on the mean-field potential for the electrons. The Woods-Saxon potential used in Ref. 13 leads to a first supershell minimum occurring for a number of electrons $N\approx 1000$, whereas the self-consistent potential used by Genzken and Brack[17] exhibits a minimum located around $N\approx 800$. Moreover, thermal effects affect shell and supershell patterns. In Ref. 17, the finite temperature of the valence electrons is included by treating the valence electrons as a canonical subsystem embedded in the heat bath of the ionic cores. Such a calculation shows that, at high temperature, thermal effects tend to smear out shell and supershell structures, whereas at low temperature the shell structure is more pronounced and additional shells in the beating region are revealed. A classical interpretation can be done assuming that the supershell pattern must not always be a simple beating of two sinusoidal waves associated with the triangular and squared trajectories. Other orbits, and the fact that each orbit can be repeated several times, have no negligible contributions on the level densities in addition to those of the two most important orbits.[16]

Experimental efforts to extend the study of clusters to large sizes have led to the observation of electronic shells in large metal clusters.[18–23] Following the procedure used first by Pedersen *et al.*[20] to display the closed-shell numbers, supershell structure has been put into evidence for sodium[20,21] and more recently for lithium clusters.[22] The beating feature was found to be dominated by contributions from the two shortest closed orbits, with the exception of the pendulating orbit.

In this paper, we present experimental evidence for thermal effects in the observation of shells and supershells in large isotopically enriched lithium clusters. In fact, among the alkalis, lithium clusters must present the most pronounced electronic shell structure, since the Fermi gas of valence electrons is confined in the smallest volume. We focus our work on cluster-size ranges located around the first node and the first antinode of the supershell pattern, and put into evidence additional structures at low temperature. Experimental results are then compared to calculations.

II. EXPERIMENT

The technique we used to reveal shell structure in lithium clusters combines photoevaporation and mass spectroscopy.

In order to avoid isotopic effect in mass spectra, we used isotopically enriched ^{7}Li metal.[24] Clusters are formed by a gas-aggregation-type source.[25] The metal is produced at a moderate pressure, a few 0.1 torr, by heating a molybdenum oven. Metal atoms effuse in a helium flow through a 4-mm hole (Fig. 1). They are carried along by 25–40 torr of helium into a 6-cm-long liquid-nitrogen-cooled copper tube. The metal clusters grow along the helium stream, which progressively cools them and dissipates their formation energy. The cluster growth stops at the end of the tube, where the metal-cluster helium mixture enters the three successive chambers of a differential pumping system. A pseudo-Gaussian-type distribution of neutral Li_N clusters is then achieved. The maximum of cluster distribution and its width are determined by the partial pressures of the me-

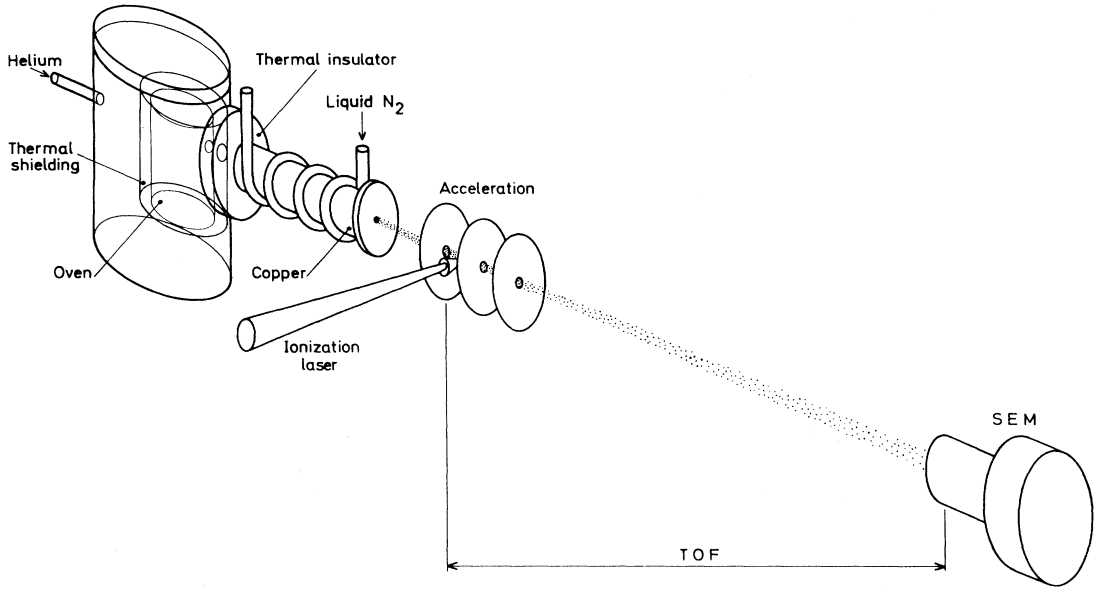

FIG. 1. Experimental setup.

tallic vapor and the carrier helium gas. Varying the metallic pressure from 5×10^{-2} to 7×10^{-1} torr promotes a shift of the maximum of the cluster distribution from $N_{\max}\approx200$ to $N_{\max}\approx1000$. Simultaneously the relative half-width $\Delta N/N_{\max}$ at half maximum increases from 0.2 to 0.6, respectively. The neutral cluster temperature depends on the cooling of helium gas, which is varied from 100 to 300 K.

The neutral clusters enter a multiplate ionizing accelerating region. Between the first two plates they are simultaneously warmed and ionized with a 10-ns, 3.50-eV light pulse provided by the third harmonic of a pulsed Nd-YAG (yttrium aluminum garnet) laser. Cluster ions resulting from ionization and evaporation after warming are accelerated before entering a time of flight where they are spatially dispersed. The length of the drift tube is 200 cm and lithium clusters are typically accelerated to 3 keV. A secondary-electron multiplier delivers ion signals averaged by a Le Croy 9400 digital oscilloscope.

It has been shown previously that the electronic structure of alkali clusters can be revealed experimentally in two ways, either through ionization or through evaporation. (i) A cold neutral cluster distribution without any previous evaporative event is ionized using light with photon energy above the ionization threshold for all clusters. Above threshold ionization, the cross section slowly varies with cluster size and the ion spectrum reflects the structureless intensities of neutral distribution. Martin shows[26] that the same neutral distribution ionized using light with energy near the ionization threshold of given clusters reveals the sharp variations in ionization cross sections near the ionization thresholds. Cluster sizes having the highest ionizing energy are seen as drops in cluster-ion mass distribution. In this case, the electronic structure of clusters is revealed through their ionization potential as drops in mass spectra. (ii) When the cluster condensation processes produce hot clusters, or if the clusters are previously warmed with a laser, subsequent evaporation and cooling occur before ionization. Following the statistic of evaporation,[7] the clusters having the highest dissociation energies slow the evaporative process down, which increases their relative intensities. Then ionization with photons having energy well above the ionization threshold of all clusters, which reflects the neutral intensities, leads to an ion distribution with maxima for the most stable clusters. The gradual increase before each maximum followed by a steep drop is typical of the electronic shell structure revealed through evaporation.

In the present experiment, a cold neutral distribution of lithium clusters previously sampled through ionization with photon energy $h\nu=4.67$ eV is ionized at several laser fluences with photon energy $h\nu=3.50$ eV. In one photon regime, a structureless cluster mass distribution is obtained with photon energy $h\nu=4.67$ eV. This characterizes cold cluster distribution ionized above the ionization threshold. With photon energy $h\nu=3.50$ eV, cluster-ion distribution presents irregularities. This photon energy, above the ionization potential of Li_N with $N\geq20$ (Ref. 27), lies in the expected energy range for the collective excitation of the valence electrons of lithium clusters, i.e., 2.58 eV for Li_8 (Ref. 28) and 4.17 eV for the macroscopic lithium sphere deduced from the volume plasmon measurement in Li.[29] For cluster sizes larger than Li_{20}, such a photon energy promotes competition between ionization and heating after the collective excitation as shown for K_n^+.[30] At high laser fluence, multistep processes can take place during the 10-ns laser-pulse duration, leading to heating of the clusters either before or after their ionization. Starting with Li_N having E_0^* as its internal energy, multistep processes taking place during the laser pulse follow the reaction paths

$$\mathrm{Li}_n(E_0^*)\rightarrow\mathrm{Li}_n(E_0^*+h\nu)\rightarrow\mathrm{Li}_n(E_0^*+2h\nu)\rightarrow\mathrm{Li}_n(E_0^*+3h\nu)\cdots$$
$$\searrow\quad\searrow\quad\searrow$$
$$\mathrm{Li}_n^+(E_0^*)+\bar{e}\rightarrow\mathrm{Li}_n^+(E_0^*+h\nu)+\bar{e}\rightarrow\mathrm{Li}_n^+(E_0^*+2h\nu)\cdots ,$$

where the solid arrows represent heating events and the dashed arrows ionizing events. After the laser pulse and before entering the accelerating region, evaporative cooling dissipates part of the internal cluster energy. For $h\nu=3.50$ eV, which is close to the energy of the plasma resonance, the probability for heating clusters is larger than the ionizing probability. However, since only ionized clusters are detected, one photon process only probes cold clusters. By increasing laser fluence, i.e., for multistep processes, the probability for ionizing "hot" clusters increases. Using a laser flux density varied between 1 μJ and 1 mJ focused on 4 mm^2, the ion-cluster mass spectra probe cluster distribution having different temperatures. However, the precise determination of cluster temperature is not straightforward, since at high laser fluence heating ionization but also evaporative cooling occur during the laser pulse. Only an estimate of the temperature range is deduced from the absorption cross section of lithium clusters[31] and the mean value of the number of atoms lost by evaporation after heating. Such a temperature is varied from a few hundred to one thousand K when the laser flux density varies from 1 μJ to 1 mJ.

III. SUPERSHELL STRUCTURE: NODE REGION

Figure 2 presents abundance distributions for lithium cluster ions $^7\mathrm{Li}_N^+$ obtained under different conditions. From the top to the bottom the laser flux density is decreased, inducing a shift of the maximum of the cluster distribution toward large masses. The top and intermediate spectra were obtained for different laser flux densities but from the same nucleation conditions, leading to a cold neutral cluster distribution peaking at $N\approx 850$. The bottom spectrum was realized from a higher mass distribution peaking at $N\approx 1150$. As shown in Fig. 2, interaction with photons having energy $h\nu=3.50$ eV provides spectra which exhibit a Gaussian-type envelope modulated by a sawtoothlike structure. For small sizes, the sawtooth behavior is attributed to peculiar stabilities for clusters having closed-shell electronic structures.[2] The shell closings are pointed like the falling edge of the sawteeth. When the sawtooth steps become more rounded, shell closings are pointed as the local maxima.

In fact, electronic shell structure results from the confinement of the electrons in a finite volume. In a semiclassical picture the quantal shell structure corresponds to the closed classical stationary orbits for the Fermi electrons. Following Balian and Bloch, the main orbits for electrons confined in a sphere are the triangular and the squared orbits.[16] Considering a metallic cluster having N atoms and N valence electrons as a sphere with radius $R=r_sN^{1/3}$, where r_s is the Wigner Seitz radius, the lengths of the main stationary paths are

$$L_3=3\sqrt{3}r_sN^{1/3} ,$$
$$L_4=4\sqrt{2}r_sN^{1/3}$$

for the triangular and squared orbits, respectively. As cluster size increases, superimposed to a smooth increasing density of states, an oscillating contribution related to a stationary path leads to shell structure. The beating pattern between the contributions of the triangular and squared orbits is called the supershell structure.[16] In a very simple way, assuming that electrons move with the Fermi velocity v_F, the Bohr's quantization along the sta-

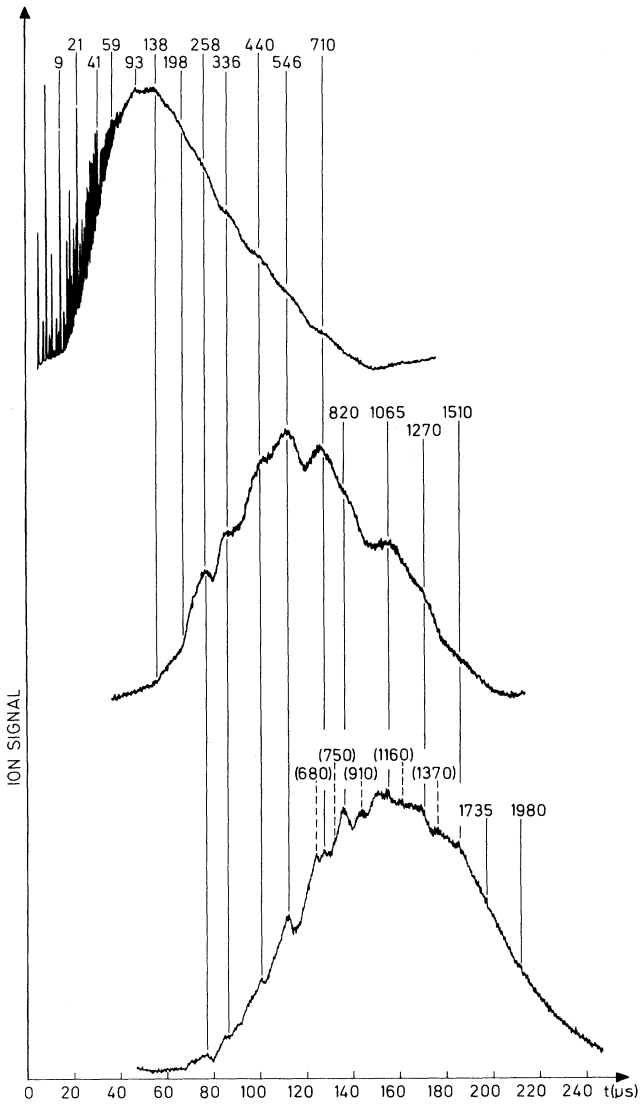

FIG. 2. Mass spectra of lithium clusters obtained after interaction with photon having energy of 3.5 eV. From top to bottom the laser flux density and consequently the cluster temperature decreases. The shell closing is clearly seen from the mass spectra. Notice that the node region of the supershell structure between $N=710$ and 1065 becomes more structured at low temperature.

tionary trajectories gives the maxima of the oscillating contributions. For the triangular orbits, the maxima occur for clusters having N_3 atoms:

$$\oint p\,dr = mv_F L_3 = mv_F r_s 3\sqrt{3} N_3^{1/3} = n_3 h \ .$$

For the squared orbits, the maxima occur for clusters having N_4 atoms:

$$\oint p\,dr = mv_F L_4 = mv_F r_s 4\sqrt{2} N_4^{1/3} = n_4 h \ ,$$

where m is the electron mass and n_3 and n_4 are integers. It should be noted that $v_F r_s$ is constant whatever the metal is, so such series are independent of the chosen alkali. Since the oscillating contribution of the level density corresponding to a single polygon has a purely sinusoidal form, the sum of the oscillating contributions of the two main orbits leads to a beating pattern. As Björnholm pointed out in his papers,[20,21] the supershell can be revealed from the plot of the cube root of the shell closing number $N_s^{1/3}$ against a running index i. The plot should be linear:

$$N_s^{1/3} = \frac{h}{mv_F r_s}\left[\frac{2}{3\sqrt{3}+4\sqrt{2}}\right] i = 0.605i \ ,$$

and a phase shift of $\frac{1}{2}i$ must occur in the node region of the beating pattern.

In Fig. 3 are plotted the cube root of the number of electrons at shell closing, from the upper and intermediate spectra of Fig. 2, against the running number i. The points (solid circles) fall on two straight lines, phase shifted by one-half the running number, putting into evidence supershell structure. As shown for sodium clusters,[20,21] the slope of the two lines 0.607 ± 0.05 coincides with the Bohr's quantization condition, but the phase shift occurs for smaller cluster sizes. More sophisticated calcula-

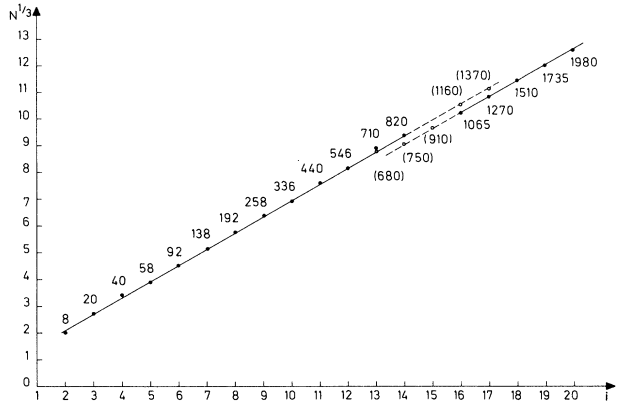

FIG. 3. Cube root of the shell closing numbers from Fig. 2 plotted against the running number i. The points fall on two straight lines phase shifted by one-half of the running number.

TABLE I. Closing-shell numbers in alkali clusters ordering according to the running number $i = l + 1$ where l is the quantum number. Experimental numbers are obtained within an error bar of few percent. Numbers in parentheses are obtained at low temperature.

	Experiment					Theory (Na)	
Shell $i = l + 1$	Li[a]		Na[b–d]		Cs[e]	Ref. 15	Ref. 17
1	2	2			2	2	2
2	8	8			8	8	8
3	20	20			20	20	20
4	40	40			40	40	34
5	58/70	58			58	58/68	58
6	92	92			92	92	92
7	138	138	138	138	138	138	138
8	198	198	198		198	198	186
9	258	263	264		263	254/268	254
10	336	341	344	335	341	338	338
11	440	443	442	440	443	440	440
12	546	557	554	555	557	562	542/556
13	710	700	680	685	700	694	676
14	(750)820	840	800	790	840	832	758/832
15	(910)		970	910		1012	912
16	1065(1160)	1040	1120	1120	1024	1100	1074/1100
17	1270(1370)	1220	1310	1370		1216/1314	1284
18	1510	1430	1500	1590		1516	1502
19	1735		1780	1810		1760	1760
20	1980		2040	2070		2048	2018
21			2370	2390		2334/2368	2328
22			2720			2672	2654

[a]This work.
[b]From Ref. 19.
[c]From Ref. 20.
[d]From Ref. 21.
[e]From Ref. 18.

tions[15,17] taking into account the mean-field potential show that the location of the minima depends rather sensitively on the kind of potential used in the calculations. Using a phenomenological Woods-Saxon potential for the valence electrons, Nishioka, Hansen, and Mottelson[15] predicted supershells of metal clusters with a node for $N \approx 1000$. The self-consistent calculations of the electronic shell and supershell structure of sodium clusters performed by Genzken and Brack,[17] employing the spherical jellium model in local-density approximation and solving by Kohn-Sham equations, predicted a node for $N \approx 800$ which is in better agreement with our experimental results for lithium clusters.

These previous calculations pointed out that thermal effects should affect the shell and supershell pattern. They predicted that the shell structure is smeared out and the amplitude of the beating pattern is reduced with increasing temperature. Moreover, the minor shells occurring in the node region vanish with increasing temperature. From Fig. 2 it can be clearly seen that our experimental results are consistent with these predictions. From the top to the bottom the laser flux density decreases, inducing a decrease of the temperature of the cluster distribution. The shell structure is sharper as temperature decreases. Moreover, at low temperature, at the bottom trace of Fig. 2, a new structure emerges in the minimum of the beating pattern (dashed lines). An interpretation can be made from the semiclassical picture. As explained in Balian and Bloch's paper, each stationary path of length L_x will give an oscillating contribution of the form $\mathrm{Im}\exp(-ikL_x)$, where the imaginary part of k produces a damping. Therefore the damping affects the shortest paths to a lesser degree. At high temperature the damping factor increases and consequently the oscillating contribution decreases. On the contrary, at low temperature the damping factor is small, and other classical orbits (especially the pentagon) can contribute to level density. Moreover the density oscillation must also be affected by repeated paths obtained by describing each orbit several times. The resulting contribution of repeated paths is a more sawtoothlike behavior for the level density than the purely sinusoidal form corresponding to one path.[16] The sum of the two sawtooth behaviors associated with the main triangular and squared orbits gives secondary maxima which are out of phase in the node region. As shown in Fig. 2 (bottom trace), experimental data are consistent with this interpretation. The corresponding points are plotted (open circles) in Fig. 3.

In Table I we compare experimentally determined shell closings for different alkalis and theoretical model predictions. As expected, the comparison shows that the position of the shell closing varies little from one element to the other. However, the small discrepancies which still exist in the experimental determination of the node supershell region may be attributed to the uncertainty of determining the shell-closing position of this region. Temperature dependence allows us to determine the main structure.

IV. ANTINODE REGION OF SUPERSHELL PATTERN

In the antinode region of the supershell pattern, the calculations of Nishioka, Hansen, and Mottelson[15] and Genzken and Brack[17] on sodium clusters do not predict any change in shell pattern with temperature except for a decrease of their relative intensity. In order to focus on this region, we modified the nucleation conditions to obtain cold neutral distributions of either sodium or lithium clusters peaking around clusters having 300 atoms.

A. Lithium case

A cold neutral lithium cluster distribution peaking at $n = 300$ with a half width at half maximum of 70 atoms interacts with photons having energy $h\nu = 3.50$ eV. The result of ionization after a slight heating is shown in Fig. 4. In addition to a well-known shell structure corresponding to the closing-shell numbers $n = 198,254,336$ (solid lines) a strong pronounced intermediate structure emerges from the mass spectrum, pointed out as dashed lines.

B. Sodium case

In order to know if this intermediate structure also occurs for low-temperature sodium clusters, we performed the same experiment with sodium. However, in the sodium case the neutral distribution is broadened as compared to the lithium case, and to clearly identify the electronic structure we recorded three spectra with photon energy $h\nu = 3.50$ eV at three different laser flux densities (Fig. 5). As explained above, in Sec. II, at high laser fluence (upper trace) the electronic structure is revealed from evaporative processes, whereas at low laser fluence (lower trace), since the ionizing photon energy lies in the ionization threshold region of small masses, the electronic structure is revealed through both the ionization threshold and slight heating processes. In a small size range, ionization threshold effects dominate, and the electronic structure is revealed as drops in the mass spectrum, whereas in a larger size range the photon energy lies well above the ionization threshold and heating

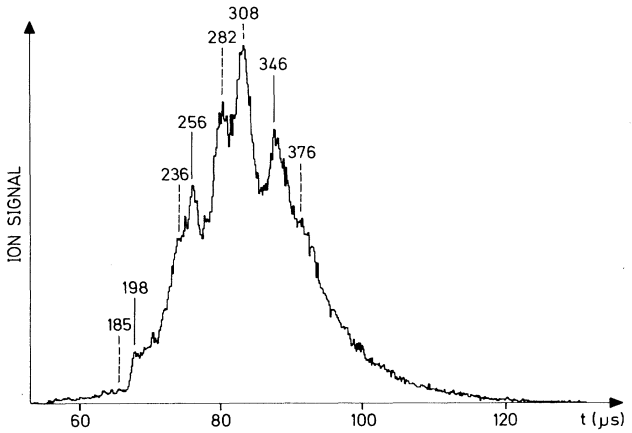

FIG. 4. Mass spectrum of lithium clusters obtained from cold neutral distribution peaking around $N = 300$, and ionized and slightly heated with photon energy $h\nu = 3.50$ eV. In addition to the shell closing peaks observed in Fig. 2 (solid marks), the intermediate structure rises (dashed marks).

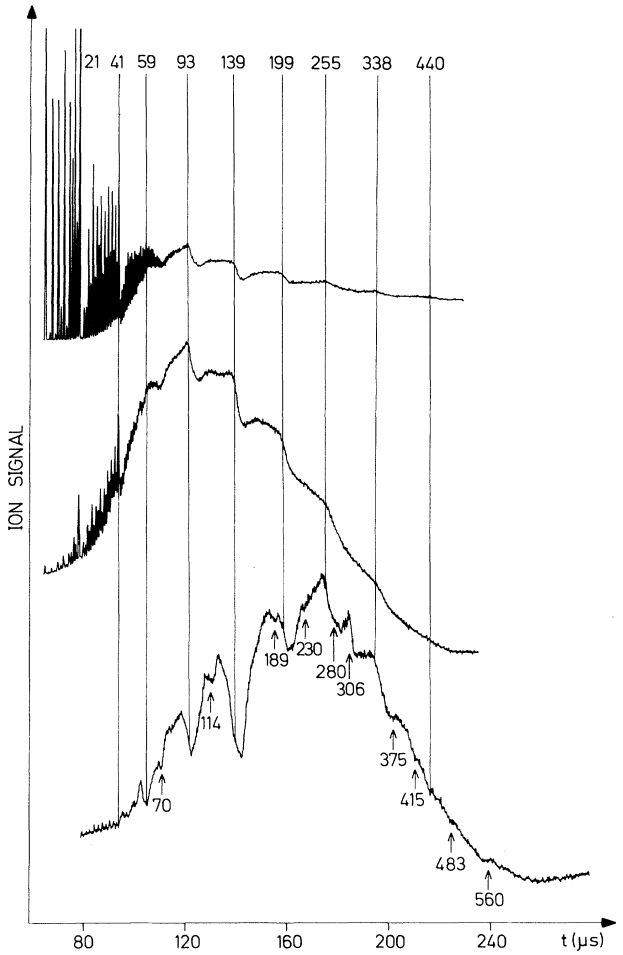

FIG. 5. Mass spectra of sodium clusters obtained after interaction with a photon having an energy of 3.5 eV. From top to the bottom the laser fluence is decreased. In the lower mass range, where the photon energy lies in the ionization threshold region of the clusters, shell structure is revealed either by photoevaporation processes (upper spectrum) or by the ionization threshold (lower spectrum). At low laser fluence the intermediate structure seen in the lithium case (Fig. 4) is also present (arrows).

effects dominate. The lower trace of Fig. 5 clearly shows, in addition to the well-known shell structure (solid lines), an intermediate structure (arrows) for numbers of atoms similar to the one observed in the lithium case.

Two possible interpretations can be given for this intermediate structure.

(i) It may be due to cluster geometry, which can affect its electronic structure, as Mansikka *et al.* calculated for icosahedral metal structures.[32]

(ii) It may be observed from the subshell electronic structure. In fact, from a self-consistent calculation using the jellium model in a local-density approximation, the

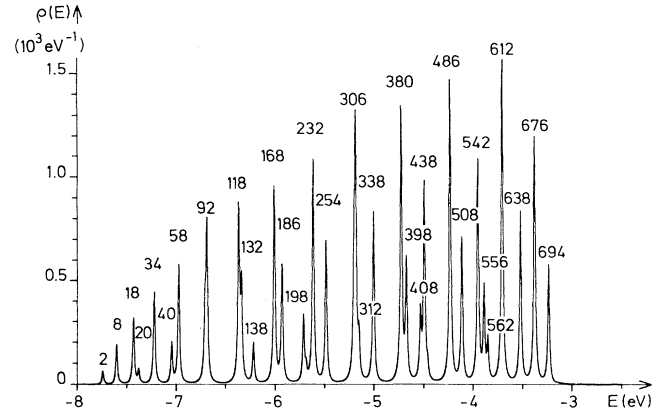

FIG. 6. Independent electron-state densities computed using the spherical jellium background model as solved self-consistently in the local-density approximation, using the program from Ref. 32 that we have modified for large masses. The Wigner-Seitz radius is taken as $r_s = 2$ Å. Notice that within experimental error in pointing out shell positions, the calculated peaks coincide with experiment in the studied antinode range $N = 93-380$.

shell structure appears as levels grouped together in energy to form shells, leaving gaps between shells. At high temperature only large gaps are observed. At low temperature smaller gaps can be seen. We have computed an independent electron-state density using a spherical Jellium background model, as solved self-consistently[33] for $N = 704$ with $r_s = 2$ Å. The result shows an ordering of subshells (Fig. 6) which can explain most of the experimental results. However, it appears from the calculation that the ordering of levels and the level grouping is very sensitive to the potential, and more refined theory is needed to totally explain the mass spectrum intensities.

V. CONCLUSION

We have investigated the electronic structure of lithium clusters for different cluster temperatures, in the size range $N = 1-2000$. As expected, the electronic structure of lithium clusters can be interpreted in a semiclassical model in terms of a beating pattern of level density due to the superposition of amplitudes associated with triangular and squared classical orbits for the Fermi electrons. We found that both orbital effects and subshell grouping are emphasized by lowering the temperature, and sharp features are revealed in the node and antinode regions of the beating pattern. Although these sharp structures can find their origin in two different physical processes, they both vanish as temperature increases. This makes very clear the location of the node region of the beating phenomenon. As expected, at higher temperature, thermal effects tend to smooth out the shell and supershell structures.

[1]W. Ekardt, Phys. Rev. B **29**, 1558 (1984).
[2]W. D. Knight, K. Clemenger, W. de Heer, W. A. Saunders, M. Y. Chou, and M. L. Cohen, Phys. Rev. Lett. **52**, 2141 (1984).
[3]W. A. Saunders, K. Clemenger, W. de Heer, and W. Knight, Phys. Rev. B **32**, 1366 (1985).
[4]M. Kappes, M. Schär, V. Röthlisberger, C. Yeretzian, and E. Schumacher, Chem. Phys. Lett. **143**, 251 (1988).
[5]W. Knight, K. Clemenger, W. de Heer, and W. Saunders, Phys. Rev. B **31**, 6360 (1985).
[6]C. Bréchignac, Ph. Cahuzac, J. Leygnier, and J. Weiner, J. Chem. Phys. **90**, 1492 (1989).
[7]C. Bréchignac, Ph. Cahuzac, F. Carlier, M. de Frutos, and J. Leygnier, J. Chem. Phys. **93**, 7449 (1990).
[8]T. Bergmann and T. P. Martin, J. Chem. Phys. **90**, 2849 (1989).
[9]S. Björnholm, J. Borggreen, O. Echt, K. Hansen, J. Pedersen, and H. D. Rasmussen, Phys. Rev. Lett. **65**, 1627 (1990).
[10]I. Katakuse, T. Ichihara, Y. Fujita, T. Matsus, T. Sakurai, and H. Matsuda, Int. J. Mass. Spectrom. Ion Process. **67**, 229 (1985).
[11]I. Rabin, C. Jackschath, and W. Schulze, Z. Phys. D **19**, 153 (1991).
[12]G. Alameddin, J. Hunter, D. Cameron, and M. Kappes, Chem. Phys. Lett. **192**, 122 (1992).
[13]M. Knickelbein, Chem. Phys. Lett. **192**, 129 (1992).
[14]J. L. Persson, R. L Whetten, Hai-Ping Cheng, and R. S. Berry, Chem. Phys. Lett. **186**, 215 (1991).
[15]H. Nishioka, K. Hansen, and B. R. Mottelson, Phys. Rev. B **42**, 9377 (1990).
[16]R. Balian and C. Bloch, Ann. Phys. **69**, 76 (1972).
[17]O. Genzken and M. Brack, Phys. Rev. Lett. **67**, 3286 (1991).
[18]H. Göhlich, T. Lange, T. Bergmann, and T. P. Martin, Phys. Rev. Lett. **65**, 748 (1990).
[19]T. P. Martin, T. Bergmann, H. Göhlich, and T. Lange, Chem. Phys. Lett. **172**, 209 (1990).
[20]J Pedersen, S. Björnholm, J. Borggreen, K. Hansen, T. P. Martin, and H. D. Rasmussen, Nature (London) **353**, 733 (1991).
[21]T. P. Martin, S. Bjornholm, J. Borggreen, C. Bréchignac, Ph. Cahuzac, K. Hansen, and J. Pedersen, Chem. Phys. Lett. **186**, 53 (1991).
[22]C. Bréchignac, Ph. Cahuzac, M. de Frutos, J. Ph. Roux, and K. Bowen, in *Physics and Chemistry of Finite Systems: From Clusters to Crystals,* edited by P. Jena *et al.* (Kluwer, Dordrecht, 1992), Vol. 1, p. 369.
[23]J. Lerme, M. Pellarin, J. L. Vialle, B. Baguenard, and M. Broyer, Phys. Rev. Lett. **68**, 2818 (1992).
[24]Isotopically enriched lithium metal ^{7}Li has been provided from Eurisotop Groupe CEA (Saclay).
[25]W. Schulze, F. Frank, K. P. Charle, and B. Tesche, Ber. Bunsenges., Phys. Chem. **88**, 263 (1984).
[26]T. P. Martin, T. Bergmann, H.Göhlich, and T. Lange, J. Phys. Chem. **95**, 6421 (1991).
[27]Ph. Dugourd, D. Rayane, P. Labastie, B. Vezin, J. Chevaleyre, and M. Broyer, Chem. Phys. Lett. (to be published).
[28]J. Blanc, M. Broyer, J. Chevaleyre, Ph. Dugourd, H. Kühling, P. Labastie, M. Ulbricht, J. P. Wolf, and L. Wöste, Z. Phys. D **19**, 7 (1991).
[29]P. C. Gibbons, S. E. Schnatterly, J. J. Ritsko, and R. J. Fields, Phys. Rev. B **13**, 2451 (1976).
[30]C. Bréchignac, Ph. Cahuzac, F. Carlier, and J. Leygnier, Phys. Rev. Lett. **63**, 1368 (1989).
[31]C. Bréchignac, Ph. Cahuzac, J. Leygnier, and A. Sarfati (unpublished).
[32]J. Mansikka, J. Suhonen, S. Valkealahti, E. Hannaren, and M. Manninen (unpublished).
[33]G. Bertsch, Comput. Phys. Commun. **60**, 247 (1990).